Bifacial, color-tunable semitransparent perovskite solar cells for building-integrated photovoltaics

Wang, Hao; Dewi, Herlina Arianita; Koh, Teck Ming; Bruno, Annalisa; Mhaisalkar, Subodh Gautam; Mathews, Nripan

2019

Wang, H., Dewi, H. A., Koh, T. M., Bruno, A., Mhaisalkar, S. G., & Mathews, N. (2020). Bifacial, color-tunable semitransparent perovskite solar cells for building-integrated photovoltaics. ACS Applied Materials & Interfaces, 12(1), 484-493. doi:10.1021/acsami.9b15488

https://hdl.handle.net/10356/142485

https://doi.org/10.1021/acsami.9b15488

Bifacial, Color-Tunable Semitransparent Perovskite Solar Cells for Building Integrated Photovoltaics

Hao Wang,[ǂ] *Herlina Arianita Dewi,*[ǂ] *Teck Ming Koh,*[ǂ] *Annalisa Bruno,**[ǂ] *Subodh Mhaisalkar,*[ǂ,§] *Nripan Mathews**[ǂ,§]

[ǂ]Energy Research Institute @ NTU (ERI@N), Nanyang Technological University, Singapore 637553

[§]School of Materials Science & Engineering, Nanyang Technological University, Singapore 639798

Corresponding Author

* annalisa@ntu.edu.sg; nripan@ntu.edu.sg,

KEYWORDS

perovskite, semi-transparent perovskite solar cell, bifacial solar cell, colorful perovskite solar cell, BIPV

ABSTRACT

Recently, semitransparent perovskite solar cells (ST-PSCs) have received overwhelming attention due to their potential applications in building integrated photovoltaics (BIPV) and in tandem solar cells. The best ST-PSCs, despite the high efficiency achieved, still show limited bifacial properties and lack aesthetic properties. Here, we have demonstrated efficient bifacial colorful ST-PSCs using copper thiocyanate (CuSCN), as hole transporting material, in a n-i-p architecture. The n-i-p ST-PSCs exhibit the highest reported bifacial factor of 93.7% and achieved a bifacial equivalent efficiency of 22.1% when illuminated under 1-sun standard conditions on the front side and with a reflected albedo of ~ 54.4% from the back side. We have also demonstrated that the colorful appearance of CuSCN based ST-PSCs can be easily tuned across the entire visible spectrum by tuning the ITO (or CuSCN) thickness without affecting their final efficiency. The wide colorful tunability and excellent bifacial photovoltaic behavior of CuSCN based ST-PSCs make them a promising candidate for BIPV applications.

INTRODUCTION

Presently, photovoltaics provide only 1% of the world energy demand. Highly efficient semitransparent solar cells, which can harvest direct as well as scattered light and can be easily integrated in the city landscapes, are strategic to maximize solar energy harvesting [1]. Integration of semitransparent solar cells in building facades, ceiling, roofs, windows, fences, walls, awnings, would be a cost-effective way to make use of buildings, increasing the total installed area in densely packed cities [2] and delivering electric energy closer to the points of demand. Currently, building ceiling and roofs are well utilized by non-transparent highly efficient crystalline silicon solar cells [1]. Semitransparent solar cells based on amorphous Si (a-Si) and polymers, have been minimally implemented [1] in windows, facades, fences, awnings also because of the limited brownish and reddish colors available. Building integrated photovoltaics (BIPV) semitransparent solar cells need to display high bifacial performance and extensive color tunabilily. Simultaneous harvesting of direct and diffused/reflected light will allow higher power conversion efficiencies (PCE) as compared to a mono-facial cell. This is important especially when semitransparent solar cells are installed on solar awnings where light can be harvested from opposite directions from sunrise to sunset and also from solar reflection albedo (RA). In addition, colourful semitransparent solar cells with broad color-tunability, which does not compromise power conversion, is important to design efficient and aesthetically appealing buildings. Scalable, efficient bifacial colorful semitransparent solar cells require three main elements: (i) extremely transparent rear electrode and interlayers to guarantee high bifacial light absorption and efficiency; (ii) good refractive index match among all the ST-SCs interlayers to create strong light interference to form distinctive colors; (iii) simple and economical fabrication process.

Perovskite solar cells (PSCs) have emerged as a key candidate for semitransparent solar cells since they are capable of achieving PCEs of over 24% [3] and 18.1% [4] for opaque and semi-transparent PSCs (ST-PSCs), respectively, with low production costs [5]. ST-PSCs have a bifacial configuration enabling the simultaneous harvesting of both direct and reflected sunlight [6]. A major challenge in realizing high-performing ST-PSCs is the replacement of opaque metal electrode with a transparent one, which allows light transmission without compromising charge collection efficiency. Recently, different strategies have been implemented to develop a good semitransparent rear electrode, including the use of thin metal layers (Au [7], Ag [8], Cu/Au bilayer [9]), silver nanowires [10], graphene [11], conductive polymers (PEDOT:PSS [12]) and dielectric/metal/dielectric multilayers [13]. The best performances so far have been achieved by using transparent conductive oxides (TCOs) such as indium tin oxide (ITO) [14], indium doped zinc oxide [4, 15] and aluminum doped zinc oxide [16]. A good combination of rear electrode and charge transport interlayers guarantees a high PCE when the ST-PSCs is illuminated from the rear side, *back* PCE [17]. As a low-cost hole transporting material (HTM), inorganic copper thiocyanate (CuSCN) is promising for bifacial ST-PSCs due to its high transparency and good chemical, structural stability [18]. CuSCN has been conventionally used below the perovskite in p-

i-n PSCs [18a, 18b, 19]. CuSCN implementation as top HTM is more challenging as it is typically dissolved in diethyl sulfide [20] or dipropyl sulfide [18a] which can damage the underlying perovskite. Recently, Arora et al. used dynamic spin coating to achieve PCE over 20 % in opaque n-i-p PSCs [20a]. Lin Fan et al. reported the only prior n-i-p ST-PSC yielding PCE of 12.47% but with just 8.74% *back PCE* due to the poor transparency of thin Au rear electrode [21].

The perception of color in PSCs can be created by modifying either their transmittance or reflectance spectrum. The few examples of colorful PSCs reported up to now are summarized in **Table S1**. Colorful opaque PSCs have been realized through the control of perovskite morphology [22], incorporation of photonic crystals [2] or ultrathin metal nano-strip optical resonators [23] and deposition of additional luminescent down-shifting layers [24]. Most of the reported colorful ST-PSCs are based on the modification of the transmission peak at specific visible wavelength to create the corresponding color. ST-PSCs realized by perovskite thickness tuning achieved color gamut only between yellow and red hues with PCEs ranging from 3.5 to 10.73% [20b, 25]. Another approach based on the inclusion of optical micro-cavities lead to the formation of distinctive transmissive colors by tuning the dielectric spacer thickness in rear electrode (Ag/WO_3/Ag [26], Ag/ITO/Ag [27]), yielding a PCE of 3.18 to 7.2%. Multi-colored ST-PSCs employing phase-compensated micro-cavities have also been demonstrated with efficiencies up to 11.18% and high angular incidence tolerance [28]. ST-PSCs with PCE of 10.12% and wide color gamut transmissive colors have been obtained using multilayer dielectric mirror (TiO_2-SiO_2) [29]. In general, despite the vivid colors that can be achieved in transmissive mode, the ST-PSCs require the perovskite layer to be very thin which compromises the final PCE. In contrast, color tuning of ST-PSCs based on the modification of the reflective spectra has less constraints on the absorber thickness. To the best of our knowledge, Jiang et al. work reported the only colorful ST-PSC obtained in pure reflection mode. The authors achieved colorful ST-PSCs with average PCEs from 11.6 to 13.8% for several visible colors by tuning the thickness of the transfer-printed PEDOT:PSS layer used as rear transparent electrodes [30]. The main limitation of this approach is that transfer-printing of a PEDOT:PSS film is a challenging and non-scalable procedure. Nevertheless, the approach of tuning the transparent electrode thickness appears to be the simplest and most effective way to tune color without introducing additional layers, extra fabrication processes or perovskite thickness variations. As a consequence this method can guarantee the most reproducible ST-PSCs' PCEs across a variety of visible colors.

Herein, we demonstrate the first bifacial colorful n-i-p ST- PSCs using CuSCN and ITO as HTM and back electrode, respectively. Indeed, the highly transparent CuSCN significantly enhanced the ST-PSCs bifacial performance, as compared to ST-PSCs based on Spiro-OMeTAD. The best CuSCN based ST-PSCs exhibited the highest reported, to the best of our knowledge, *front* PCE of 14.2% when illuminated from the front side and *back* PCE of 13.3% when illuminated from the back side. Bifacial factor is commonly used to evaluate the bifacial efficiency of a ST-SC. It is defined as the ratio of back and front side PCEs measured from each sides independently under standard 1-sun illumination.[31] These CuSCN ST-PSCs achieve the highest reported bifacial factor of 93.7% for n-i-p ST-PSCs. The ST-PSCs achieved a *bifacial*

equivalent efficiency of 22.1%, when illuminated under 1-sun on the front side and ~50% rear albedo from the back side. The color generation capability of the CuSCN based ST-PSCs was first investigated theoretically by optical simulation to serve as design guideline and then proved experimentally. CuSCN based ST-PSCs showed tunable distinctive visible colors by simple ITO-thickness tuning, without a power conversion efficiency compromise. The color tunability could be very beneficial for BIPV application to design aesthetically appealing buildings.

RESULTS

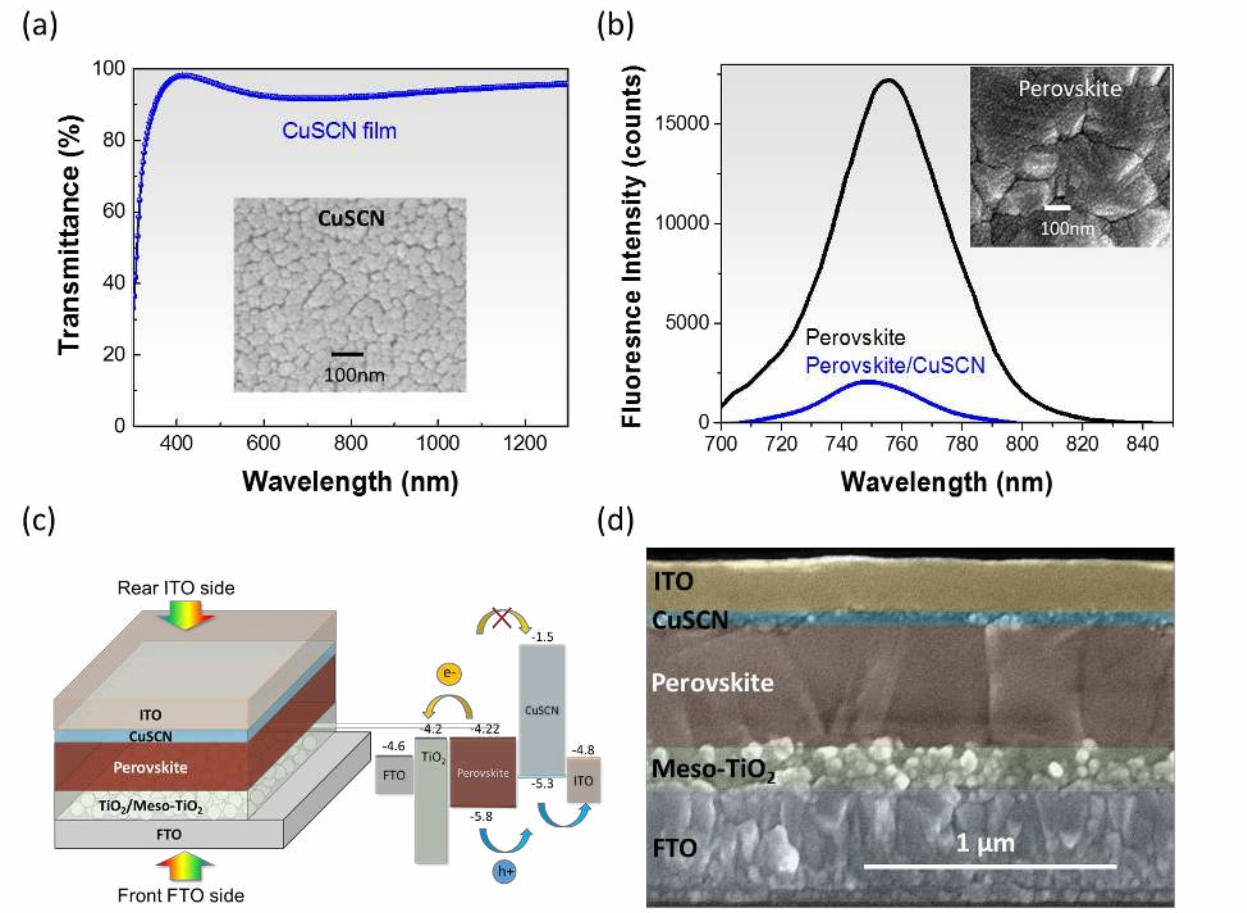

Figure 1: **ST-PSC structures and interlayers characteristics**. (a) Transmittance spectra of CuSCN film on glass. Inset shows the morphology of CuSCN films. (b) Steady-state photoluminescence spectra of perovskite films and triple-cation perovskite/CuSCN bilayer on glass substrates. Inset shows the morphology of perovskite films. (c) Structure of bifacial ST-PSCs and energy band alignment of the interlayers. The high CuSCN LUMO level (-1.5 eV) efficiently blocks electrons at the HTM/perovskite interface. (d) Cross-sectional FESEM image of bifacial ST-PSCs.

CuSCN film has an average transparency above 93% between 300 nm and 1300 nm (**Figure 1a**), which makes it an excellent HTM for bifacial ST-PSCs. This transparency is considerably wider and higher compared to the Spiro-OMeTAD one (Figure S1). The CuSCN film, inset of **Figure 1a**, displays a grainy morphology with an average grain size of 30-50 nm, in agreement with previous reports.[18b, 18c] Steady-state photoluminescence (PL) spectra of the triple-cation perovskite $[Cs_{0.05}(MA_{0.17}FA_{0.83})_{0.95}\ Pb(I_{0.83}Br_{0.17})_3]$ pristine film and the perovskite/CuSCN bilayer (**Figure 1b)**, show a significant reduction of the perovskite PL intensity when coated with CuSCN. The quenching efficiency is ~90 %, comparable to the one produced by Spiro-OMeTAD (Table S2) suggesting a similar ability to charge extraction [20a], although other reasons for PL reduction could be related to non-radiative defects at the interfaces. This combined with the high optical transparency make it a promising HTM for bifacial ST-PSCs.

The bifacial mesoporous n-i-p ST-PSCs (glass/ fluorine-doped tin oxide (FTO)/compact-TiO_2/mesoporous TiO_2/perovskite/CuSCN/ITO) is illustrated in **Figure 1c**, with the energy level positions of different interlayers measured by photon electron spectroscopy in air (PESA). The active layer is triple-cation perovskite with a bandgap of ~1.58 eV [32], which can guarantee high stability, good and reproducible performances. The cross-sectional FESEM image of ST-PSCs architecture is shown in **Figure 1d** with perovskite and CuSCN thickness of ~ 500 nm and ~ 50 nm, respectively. The semitransparent ITO electrode was deposited directly on top of CuSCN using DC sputtering [14f] without any buffer layer. ST-PSCs illuminated from FTO electrode, achieved a *front* PCE of 14.2% with V_{oc} of 0.978 V, J_{SC} of 20.2 mA/cm^2, fill factor (FF) of 72.1% (**Figure 2 a**). This is the highest PCE reported for CuSCN based ST-PSCs in the n-i-p configuration. The V_{oc} close to 1 V indicates negligible damage to the perovskite surface during the ITO sputtering deposition. All the photovoltaic parameters strongly outperform ST-PSCs employing Spiro-OMeTAD and polytriarylamine (PTAA) as HTM without buffer layer (Figure S3). These results reveal the structural robustness of CuSCN to the ITO sputtering which makes it suitable for buffer layer-free ST-PSCs. J-V characteristic of CuSCN based ST-PSCs illuminated (under 1-sun) from rear ITO electrode, **Figure 2a**, show a very small J_{sc} reduction of ~1.2 mA/cm^2 and unchanged V_{oc} (0.974 V) and FF (72.0%) values, as compared to front illumination, resulting in a *back* PCE of 13.3%, **Table 1**. Our CuSCN based ST-PSCs have a very high bifacial factor of 93.7%, indicating excellent light harvesting capability from both sides thanks to the very low parasitic absorption of both the electrodes and charge transport layers [33]. The narrow *front* and *back* PCEs distributions for CuSCN based ST-PSCs also confirmed the good reproducibility of the fabrication process (Figure S4). J-V characteristics of CuSCN based PSCs as a function of light intensity (Figure S5) showed linear photovoltaic behavior, indicating the absence of significant energy barrier within the PSCs.

Table 1: Photovoltaic characteristics of bifacial CuSCN based ST-PSCs.

Illumination side	**V_{OC} (V)**	**J_{SC} (mA/cm^2)**	**FF (%)**	**PCE^{max} (%)**	**PCE^{ave} (%)**

front-FTO	0.978	20.2	72.1	14.2	13.7 ± 0.3
rear- ITO	0.974	19.0	72.0	13.3	12.7 ± 0.6

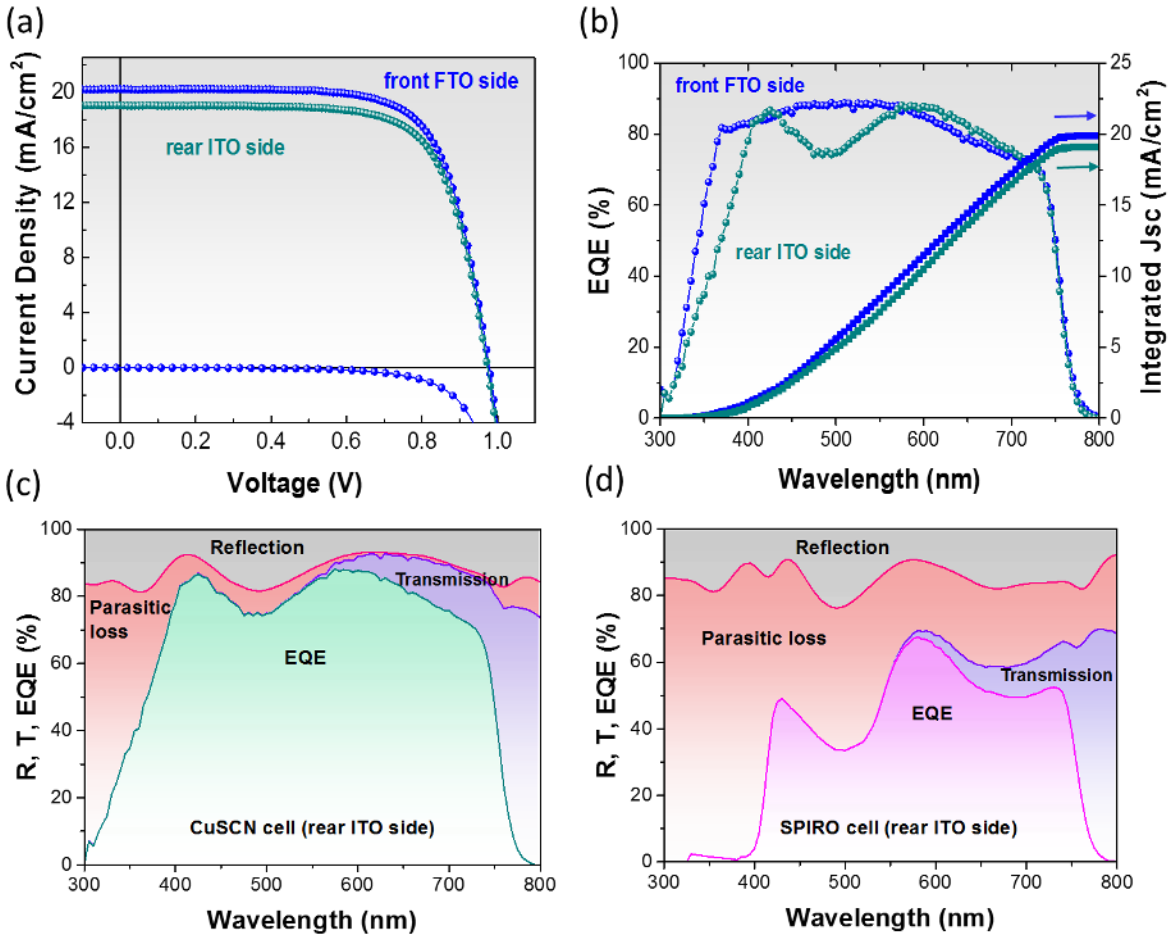

Figure 2: **Bifacial ST-PSC photovoltaic characteristics under 1 sun illumination through FTO and ITO side**. (a) Current-voltage (J-V) curves in dark and under illumination; (b) EQE spectra and integrated current density. (c) Optical analysis of the CuSCN ST-PSCs and their integrated current density (calculated for λ=300-800 nm): EQE spectra (19.10 mA/cm^2), reflection (3.27 mA/cm^2), transmission (3.62 mA/cm^2) and parasitic absorption losses (1.50 mA/cm^2) in bifacial cells based on CuSCN as HTM using directly sputtered ITO as electrode. (d) Optical analysis of the Spiro-OMeTAD ST-PSCs and their integrated current density (calculated for λ=300-800 nm): EQE spectra (11.50 mA/cm^2), reflection (4.14 mA/cm^2), transmission (3.05 mA/cm^2) and parasitic absorption losses (8.79 mA/cm^2) in bifacial cells based on Spiro-OMeTAD as HTM using 1nm Ag as buffer layer and ITO as rear electrode when illuminated from the rear ITO side.

External quantum efficiency (EQE) spectra for the best performing ST-PSC reaches 85 – 89% in the spectral range of 360-640nm with an integrated current density of 19.91 mA/cm^2

when illuminated through the front FTO side **(Figure 2b)**. The EQE drop in 550-800 nm region is mainly due to unabsorbed light transmission through the rear ITO transparent electrode (Figure S6). Similarly, with back illumination, the EQE is above 80% in the visible range leading to a high integrated back J_{sc} of 19.1 mA/cm^2. This is much higher than the previously reported back J_{sc} and EQE for ST-PSCs [8b, 9, 12, 15b, 21, 33]. Instead, the drop around 480 nm is due to the higher reflection loss from the ITO side as compared with the FTO side (**Figure 2c** and Figure S6). To analyze in detail the different contributions to the photocurrent losses for the rear ITO illumination, we plot the back-EQEs together with the light reflection and the overall CuSCN ST-PSC transmission at the ITO side (**Figure 2c**). The detailed optical analysis show that the main losses in the EQE comes from the reflection loss, consequently the J_{sc} can be further improved by tuning the ITO thickness and applying antireflection coatings. The parasitic losses due to CuSCN/ITO rear electrode are very low due to the high transparency of CuSCN and ITO (Figure S7). In comparison, a Spiro-OMeTAD based n-i-p ST-PSC was also fabricated according to our previous structure [14f] and its photovoltaic parameters are presented in Figure S8. The Spiro-OMeTAD based ST-PSC back-EQE is significantly lower than CuSCN based ST-PSC, due to high parasitic absorption in doped Spiro-OMeTAD HTM and the thin Ag buffer layer required to protect the Spiro-OMeTAD. (**Figure 2d**).

As mentioned earlier, bifacial ST-SCs can outperform mono-facial SCs through harvesting of the reflected sunlight through the rear ITO side [6b] (**Figure 3a)**. The bifacial solar cell can be characterized by the *bifacial equivalent efficiency*, equal to the efficiency of a regular mono-facial solar cell which is able to generate the same power per unit area as the bifacial cell at the same test conditions. This is practically equal to the sum of the front side efficiency, and the rear side efficiency multiplied by the proportion of irradiance on the rear side [31]. The total additional power that can be gained is determined by the *back* PCE and the rear albedo from the background. Common backgrounds have very different RA ranging from approximately 30% for earth and grass, 60% for white concrete, and 90% for snow [6b, 6c]. To investigate the bifacial performances, the best performing bifacial ST-PSC is tested by using a *white paper* (*PaperOne copier* A4) as a back reflector to simulate the light RA. The experimental details are reported in Experiment Section and **Table S3**. The bifacial ST-PSC J-V performances, measured with standard 1-sun illumination at the front FTO side and with back reflection with RAs of ~33.7% and ~54.4% are reported in **Table 2** and **Figure 3b**. For 54.4% RA, a champion *bifacial equivalent efficiency* of 22.1% has been achieved. Considering that the bifacial ST-PSC will perform linearly with both side illumination, we calculated the projected *bifacial equivalent efficiency* under various RAs, **Figure 3c**. A *bifacial equivalent efficiency* of 18.2% and 26.2% could be achieved with earth (RA of 30%) and snow (RA of 90%) backgrounds, respectively. The measured *bifacial equivalent efficiencies*, with RAs of ~ 33.7% and ~ 54.4% **Figure 3c**, show a very good match with the projected calculation. Thus, the overall ST-PSC efficiency can be enhanced with increased background RA, indicating CuSCN ST-PSC is an excellent bifacial cell.

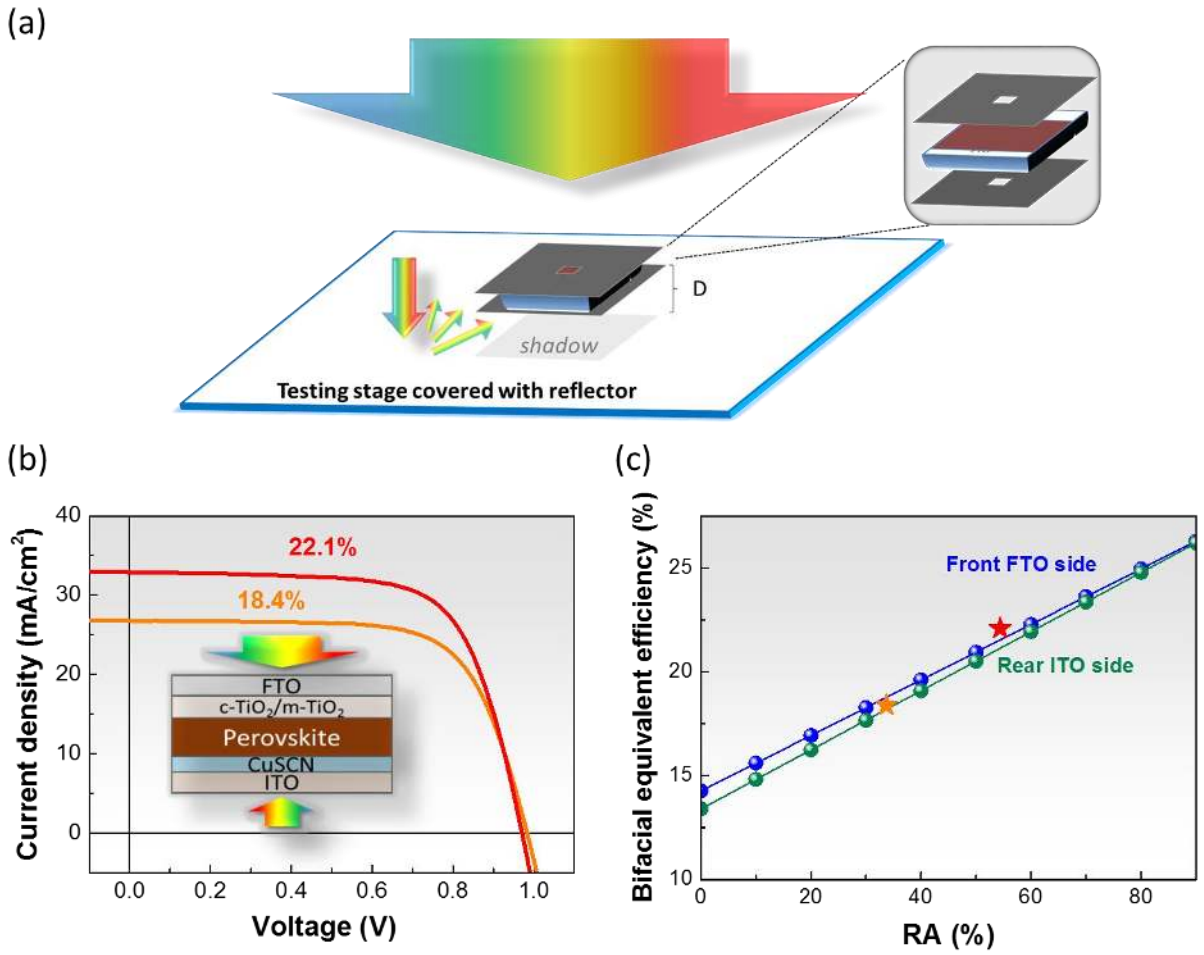

Figure 3: (a) Schematic of the measurement set-up for the bifacial CuSCN ST-PSC harvesting light from both front side direct 1-sun illumination from solar simulator and the reflection (or scattered) light (reflection albedo) from the background. A white paper is used as back reflector to enhance the background reflection albedo (RA). The ST-PSC to stage distance (D) can be varied to adjust the shadowing effect to vary the RA. (The details of bifacial measurement is explained in the Experimental Methods.) (b) Current-voltage characteristics of the bifacial ST-PSC when illuminated using the set-up described in (a), with front direct 1-sun illumination and back RA of 33.7% (orange curve) and 54.4% (red curve). (c) Calculated prediction of *bifacial equivalent efficiency* of bifacial ST-PSCs with different RA (Blue and Cyan dots connected with lines). The "orange star" and "red star" represent the experimental measurements with 33.7% RA and 54.4% RA.

Table 2: Bifacial Photovoltaic parameters of CuSCN bifacial ST-PSCs with front illumination (standard 1 sun) and back reflection.

With white paper as back reflector	V_{OC} (V)	J_{SC} (mA/cm^2)	FF (%)	Bifacial Equivalent Efficiency (%)
33.7% RA	0.983	26.8	69.8	18.4
54.4% RA	0.971	32.9	69.1	22.1

BIPV requires efficient bifacial and colorful ST-PSCs to be able to maximize the solar harvesting area (and in turn the energy power supply) to realize aesthetically appealing designs. Colorful PSCs, should be able to cover a wide range of colors without compromising the power conversion efficiency. To attain this goal, we modulated the optical reflection spectra of the ST-PSCs from the ITO electrode side to form different reflective colors. The light reflection spectra can be tuned by controlling the light interference effects arising from the coherent superposition of reflected and transmitted electromagnetic fields generated at the multiple interfaces in the ST-PSCs [30]. The CuSCN based ST-PSCs optical properties were simulated using Finite Element Method (FEM) [34] (details in Experiment Section), determining the effect of both ITO and CuSCN thicknesses on the reflectance spectra and CIE 1931 color coordinates for various ITO/HTM conditions (Figure S9 and **Figure 4** respectively). The color gamut generated by the ST-PSCs color gamut for different ITO thickness, and fixed CuSCN thicknesses of 50 nm and 110 nm are shown in **Figure 4a** and **Figure 4b** respectively. In both cases, excellent color tunability across entire visible spectrum can be achieved by just changing the ITO thickness. For CuSCN=50 nm, the color hues are distinctive with strong reflection peaks (Figure S9a) due to the strong light interference effect for thin layers. As CuSCN thickness increases to 110 nm, the ST-PSCs exhibit similar contour pattern, but with weaker color hues due to the smaller reflection peaks (Figure S9b). The ST-PSCs CIE coordinates with other CuSCN thicknesses (30 nm, 80 nm, 150 nm) have also been investigated and reported in Figure S10. **Figure 4c** and **Figure 4d** shows the ST-PSC colors obtained by changing the CuSCN thickness while keeping the ITO thickness fixed either at 100 nm or 200 nm. In the first case, ST-PSCs also are able to generate colors almost across entire visible spectrum by varying the CuSCN thickness, while for ITO = 200 nm, it is not possible to achieve blue or purple color by only tuning CuSCN thickness.

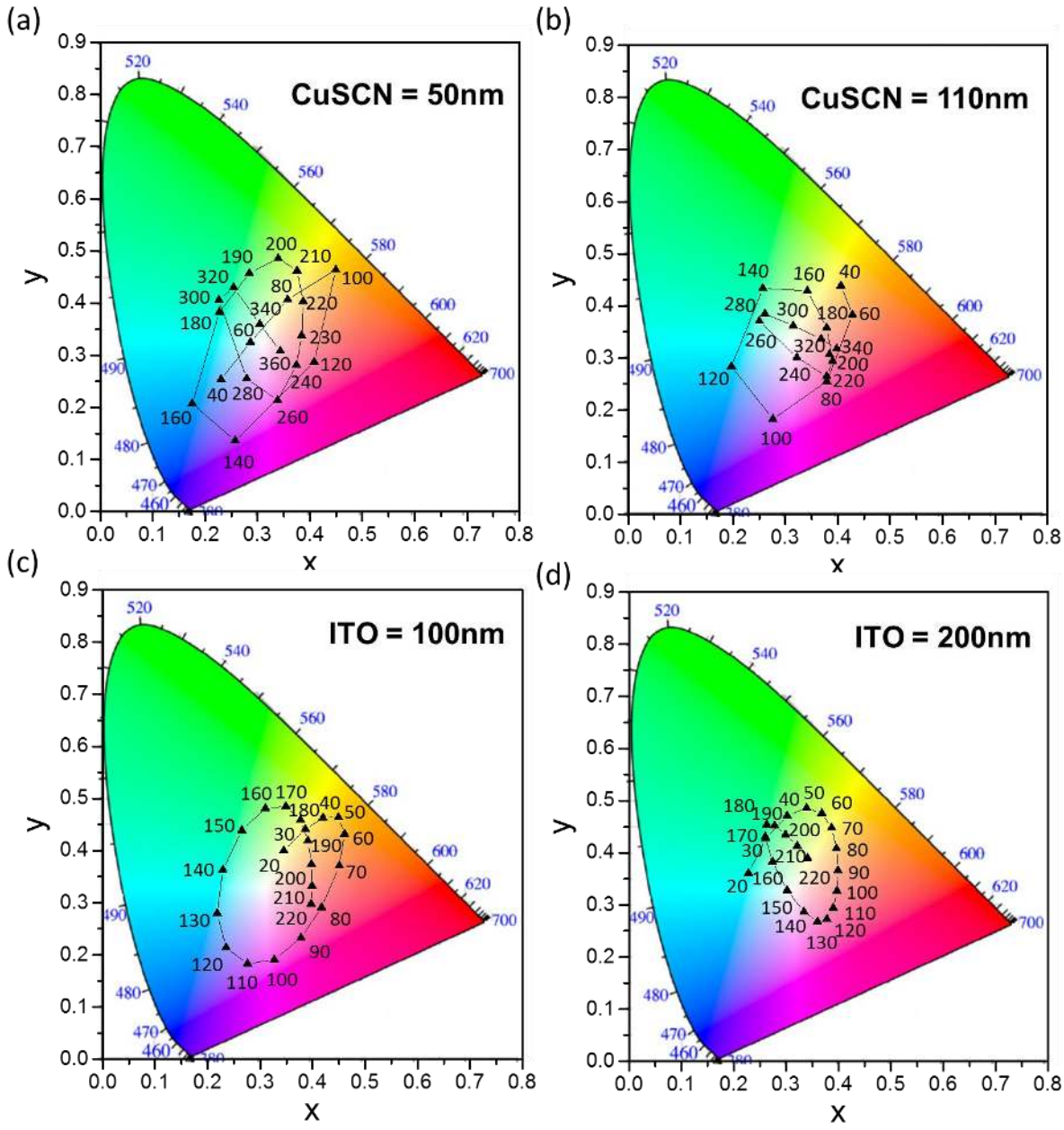

Figure 4 Color coordinates (x, y) representation in the CIE 1931 chromaticity diagram of optical simulated light reflectance spectra of CuSCN based bifacial ST-PSCs from ITO electrode side based on a fixed bottom layer stack: FTO (400 nm)/TiO_2(50 nm)/Perovskite(500 nm)/CuSCN/ITO. (a) CuSCN = 50 nm, with different ITO thickness. (b) CuSCN = 110 nm, with different ITO thickness. (c) ITO = 100 nm, with different CuSCN thickness. (d) ITO = 200 nm, with different CuSCN thickness.

Following the results of our optical study we were able to design colorful bifacial CuSCN based ST-PSCs by varying the ITO thicknesses. ST-PSCs which do not compromise their efficiency by changing the color are challenging to be realized since light loss due to color reflection and series resistance increase in thin ITO electrodes are difficult to overcome. **Figure 5a** shows the photo of colorful ST-PSCs with different ITO thickness varying from 105 nm to 320 nm while keeping the CuSCN thickness at 50 nm. Photos of same ST-PSCs taken against indoor light are also shown in Figure S11a. ST-PSCs can be tuned to produce distinctive colorful hues across entire visible light spectrum as light-green, orange, pink, violet, blue, deep-green, yellow. Their corresponding CIE 1931 color coordinates are reported in **Figure 5b** and Table 3. **Figure 5c** and Figure S11 show the reflectance spectra of all the CuSCN ST-PSCs probing that the strength and the position of the refractive peaks can be effectively modified by simple tuning the ITO thickness. Very interestingly, all the colorful CuSCN based ST-PSCs show very consistent photovoltaic parameters for varying ITO thicknesses, **Table 3** and Figure S12**.** Blue and green ST-PSCs, which are also the most desired for the BIPV [2] applications are the best performing ones with PCE above 13%. The light green ST-PSC, with the thinnest ITO of ~105 nm, can still deliver an efficiency of ~11.2% (Figure S12 and **Table 3**). The PCE drop is mainly due to the FF decrease due to the increased series resistance of the thinner ITO, which can be reduced by incorporating metal grids on top of ITO electrode. On the other hand, for all the colorful ST-PSCs, the bifacial J_{sc} is very high (18 to 19 mA/cm^2), confirming that the light reflection loss are always very small for all the ITO thickness investigated.

The transparency of the ST-PSCs is another critical property required by a variety of different BIPV applications. High average visible transmittance (AVT, >20% [1, 35]) is required for solar window applications to allow enough visible light to pass through to provide visual comfort, while high infrared (IR) transmittance (~80%) is required if the ST-PSC is stacked on top of other lower bandgap solar cells to form tandem solar cells. In this work, we used a perovskite absorber with medium thickness of ~500 nm to develop the CuSCN ST-PSC for BIPV applications and study its bifacial performance and color tunability. The transmission spectra of the CuSCN ST-PSCs for two different ITO thickness (130 nm and 210 nm) are presented in Figure S13. For applications requiring higher AVT, a much thinner perovskite layer will be needed to enhance the light transmission in visible region.

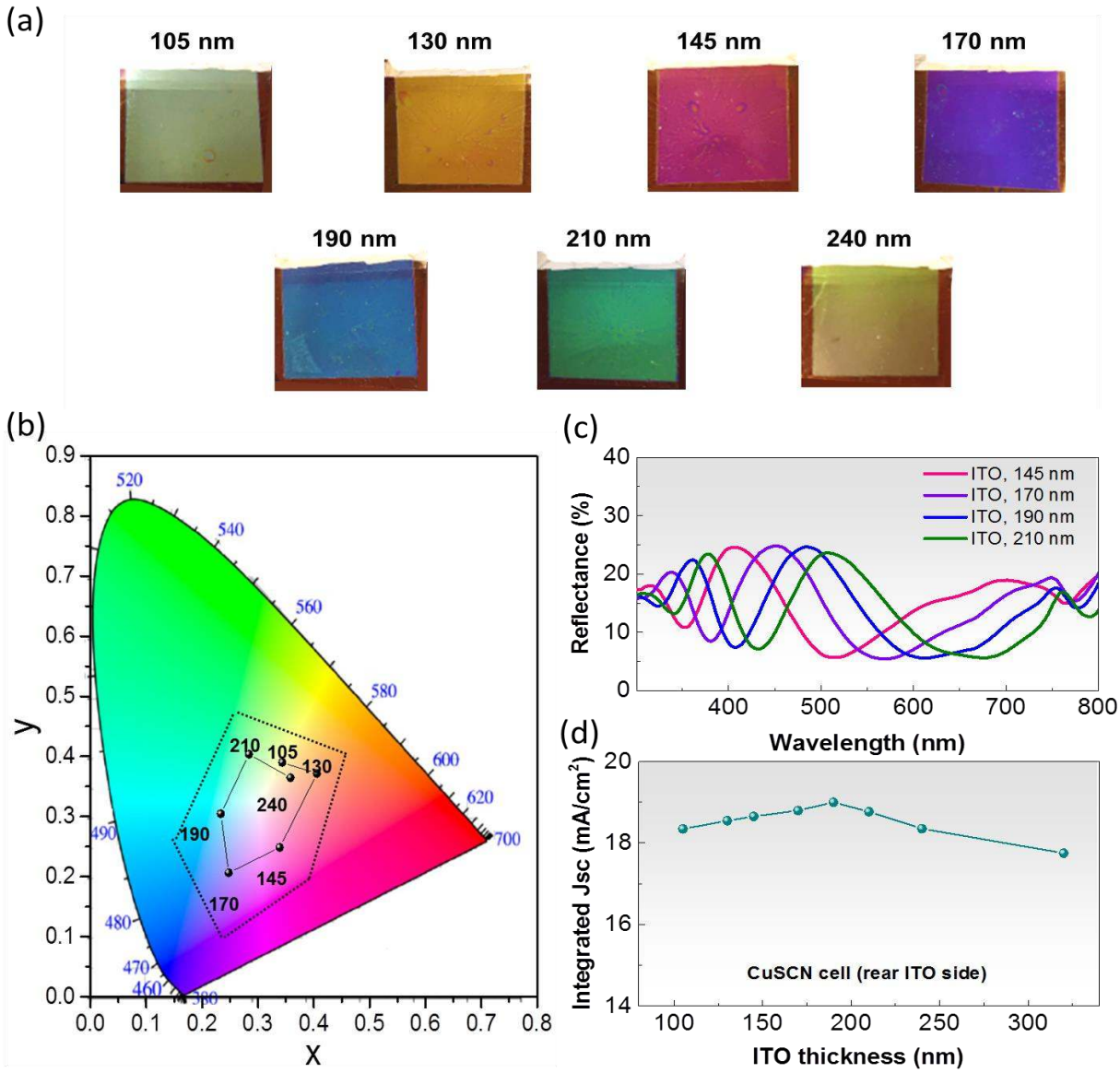

Figure 5: (a) Photographs of CuSCN based ST-PSCs from ITO electrode side with distinctive colors. (Device structure: FTO/c-TiO_2/m-TiO_2/perovskite/CuSCN/ITO; ITO thickness is varied from 105 nm to 240 nm). (b) Color coordinates (x, y) representation of the colorful CuSCN based ST-PSCs with different ITO thickness in the CIE 1931 chromaticity diagram (c) Reflectance spectra of CuSCN based ST-PSCs with pink, purple, blue and green color when ITO thickness is about 145 nm, 170 nm, 190 nm and 210 nm, respectively. The reflectance spectra of the ST-PSCs with additional ITO thicknesses are presented in Figure S11b. (d) Integrated J_{sc} calculated from back-EQE spectra (from rear ITO side) for CuSCN based ST-PSCs with different ITO thicknesses.

Table 3: *Back* PCEs (colorful side) of CuSCN based bifacial ST-PSCs with illumination from ITO side under standard 1 sun illumination.

Color	ITO thickness (nm)	CIE 1931 (x,y)	V_{OC} (V)	J_{SC} (mA/cm^2)	FF (%)	PCE^{Champ} (%)	PCE^{ave} (%)
Light Green	105	(0.34, 0.39)	0.930	18.4	65.5	11.2	11.0 ± 0.2
Orange	130	(0.41, 0.37)	0.930	18.7	61.2	10.6	10.0 ± 0.7
Pink	145	(0.34, 0.24)	0.947	18.2	64.1	11.1	10.9 ± 0.2
Violet	170	(0.25, 0.20)	0.948	18.8	69.0	12.3	11.9 ± 0.5
Blue	190	(0.23, 0.30)	0.974	19.0	72.0	13.3	13.0 ± 0.3
Green	210	(0.28, 0.41)	0.981	18.7	72.0	13.2	12.9 ± 0.2
Yellow	240	(0.36, 0.36)	0.974	18.4	72.4	13.0	12.6 ± 0.3

CONCLUSION

In conclusion, we have demonstrated efficient bifacial colorful ST-PCSs using inorganic CuSCN as HTM and by tuning the ITO electrode thickness. CuSCN's low parasitic absorption in the visible region leads to excellent back performance and ST- PSCs with bifacial equivalent efficiency of 22.1% with simultaneous 1-sun front illumination and RA of 54.4% on the back side. A bifacial equivalent efficiency of over 26% can be achieved with high background reflection albedo of 90%. These properties make our ST- PSCs suitable in applications which present strong background RA such as awnings. Moreover efficient colorful CuSCN ST-PSCs with large color tunability across visible spectrum have been realized by employing straightforward tuning of the ITO electrode thickness. The efficiency of the methodology has been proven both theoretically and experimentally. Our results clearly indicate that bifacial colorful CuSCN based ST-PSC is a very promising candidate for BIPV applications.

EXPERIMENTAL METHODS

Semi-Transparent Perovskite Solar Cell Fabrication

Fluorine doped tin oxide (FTO) glass substrates (Tec15) were cleaned by ultra-sonication in a decon soap solution followed by deionized water and ethanol. The cleaned substrates were then treated under air plasma for 5min prior to usage. Compact TiO_2 (c-TiO_2) was spray deposited at 500°C on a hotplate, using titanium diisopropoxide bis (acetylacetonate) (Sigma-Aldrich, 75 wt% in isopropanol) mixed with isopropanol (Sigma Aldrich, anhydrous) and acetylacetone (Sigma Aldrich). For the Mesoporous TiO_2 (mp-TiO2) layer, Dyesol 30NRD was diluted in absolute ethanol in the ratio 1:5.5 (w/w) and then spun onto the substrate at 5500 rpm for 30s. The substrate was then sintered at 500°C for 15 min. Before solar cell fabrication, 10mg/mL lithium bis(trifluoromethylsulphonyl) imide solution in acetonitrile (Sigma Aldrich, anhydrous) was spun on at 3000rpm for 20s and annealed at 450°C for 30 min.

1.5M triple cation perovskite precursor solution, $Cs_{0.05}(MA_{0.17}FA_{0.83})_{0.95}Pb(I_{0.83}Br_{0.17})_3$, was prepared by dissolving MABr (Dyesol), $PbBr_2$ (TCI), FAI (Dyesol), PbI_2 (TCI) inside a mixture of DMF and DMSO at a ratio of 4:1 (v/v) at room temperature for 1h. CsI in DMSO was added into the perovskite precursor solution to form the composition required. The dissolved perovskite solution was spin-coated on mp-TiO_2 layer first at 1000 rpm for 10 sec followed immediately by 6000 rpm for 17s. Simultaneously, 0.1mL dichlorobenzene was dripped onto the substrate at 13s. The film was then heated at 100°C for 1h in order to obtain black and dense perovskite film. On top of the perovskite layer, a solution of Spiro-OMeTAD (70mg/mL in chlorobenzene), with additional 4-tert-butylpyridine, lithium bis (trifluoromethylsulphonyl) imide (520mg/mL in acetonitrile (ACN)) and FK102 (17.2mg/50 mL of ACN) was spin-coated at 5000rpm for 30s. CuSCN was dissolved in Diethyl sulfide solvent with a concentration of 30 mg/mL and stirred for 20 min and then dynamically spin coated on perovskite layers (spinning then dropping) at 5000 rpm for 30 sec. This method allows mitigation of the chemical damage to bottom perovskite caused by Diethyl sulfide. All the perovskite and HTM preparations were done inside glovebox. The samples were then annealed on hotplate at 60 °C for 8 min. The post anneal process could help evaporate the solvent faster to minimize the exposure time of perovskite to Diethyl sulfide and promote solid film formation

For the best performing CuSCN based semi-transparent PSCs, ~ 190 nm indium tin oxide (ITO) was directly deposited using DC sputter at 25 W power for 80 min, to form a transparent electrode. The Ar and O_2 gas flow rate was 30 and 0.6 sccm respectively. For the fabrication of colorful ST-PSCs, the ITO thickness was tuned by controlling the ITO deposition time and then the thickness was measured by Scanning Electron Microscope (SEM). For Spiro-OMeTAD based PSCs prior to ITO deposition, a buffer layer of thin Ag was thermal evaporated to protect Spiro-OMeTAD and perovskite.

Thin Film and Device Characterizations

Transmission (T) spectra of the thin films were recorded using UV-Vis-NIR Spectrophotometer (UV3600, Shimadzu) equipped with an integrating sphere. Top view and cross section images of the SCs were recorded using a Field Emission Scanning Electron Microscope (FESEM, JEOL, JSM-7600F, 5kV and 10mA). A thin layer of Pt was coated on top

of the samples to avoid charging effect. Thin films were also characterized by X-ray diffraction (Bruker D8 Advance). Steady state photoluminescence spectra were measured using a table-top Fluoromax-5 system. Photocurrent-voltage characteristics of perovskite SCs were recorded by applying an external potential bias to the cells while recording the generated photocurrent with a digital dual source meter (Keithley 2612 sourcemeter). The J-V measurements were performed using San-EI Electric, XEC-301S solar simulator under standard simulated AM1.5G illumination and the light intensity was calibrated using standard reference silicon cell. The EQE was determined using a PVE300 (Bentham), with a dual xenon/quartz halogen light source and measured in DC mode without additional light bias. The light intensity was calibrated using a silicon calibrated detector (Newport). An aperture mask with dimensions 0.3x0.3 cm^2 was used for Perovskite J-V.

Bifacial Performance Testing

For bifacial performance testing, the ST-PSC is placed at an elevated level to the testing stage. The ST-PSC device substrate is small with a dimension of 2.2 cm ×2.2 cm, which is covered with metal mask on both sides to define the active area of 0.16 cm^2. The region underneath the ST-PSC will have a dark shadow when illuminated by the 6 inch square beam from the solar simulator. A large portion of light will reach the testing stage and will be reflected back. Part of the reflected light (reflection albedo) can reach the rear side of the ST-PSCs and be absorbed. By adjusting the device to stage distance, the shadowing effect underneath the ST-PSC and the amount of reflection albedo reaching the rear side will be affected. A white paper is used as reflector to enhance the light reflection albedo. We measured the bifacial ST-PSC performance with simultaneous front direct 1-sun illumination and back reflection from white paper background with a device to stage distance (D) of ~1.5 cm; and D of ~ 3 cm, to adjust the shadowing effect and maximize the background RA. The reflected background intensity was measured (Table S3) by using a power meter for D=1.5 cm and D=3 cm. The ratio of these values and light intensity measured under standard 1-sun illumination represent the reflection albedo (RA) ratio. RA of ~33.7% and 54.4% were obtained for D=1.5 cm and D=3 cm, respectively.

Optical Simulation

Optical simulation was carried out using Finite Element Method (FEM) [34]. The simulated structure consists of an n-i-p structure perovskite ST-PSC consisting of FTO/TiO_2/$CH_3NH_3PbI_3$/CuSCN/ITO. The bottom layers were kept unchanged as FTO (400nm)/TiO_2(50nm)/$CH_3NH_3PbI_3$(500nm). CuSCN layer thickness or ITO thickness was varied to study its effect on the color generation and light absorption. Light with wavelength ranging from 300 to 1200 nm was incident normal to the ITO top layer of the ST-PSC. The optical characteristics including light reflection, absorption, and transmission were extracted from the simulated spatial distribution of energy flux in the ST-PSC structure simulated. The refractive index value of FTO [36], TiO_2 [36], $CH_3NH_3PbI_3$ perovskite [37], CuSCN [38], ITO [39] were extracted from literature.

ASSOCIATED CONTENT

Supporting Information. This material is available free of charge via the Internet at http://pubs.acs.org.

Table S1: Summary of reported colorful PSCs. Figure S1: Transparency of Spiro-OMeTAD, steady-state PL of perovskite/Spiro-OMeTAD. Table S2: quenching PL efficiency. Figure S2: SEM of CuSCN coverage. Figure S3: J-V curves of Sprio-OMeTAD/PTAA ST-PSCs without buffer. Figure S4: Efficiency statistics. Figure S5: Light intensity dependence. Figure S6: Optical analysis for front FTO side. Figure S7: Absorption spectrum of ITO film. Figure S8: J-V curves and EQE of Sprio-OMeTAD ST-PSCs with thin Ag buffer. Table S3: reflection albedo evaluation details. Figure S9: Reflection spectra of simulated ST-PSCs. Figure S10: CIE 1931 coordinates of ST-PSCs. Figure S11: Photographs and reflection spectra of CuSCN ST-PSCs. Figure S12: EQEs & J-V curves for different ITO thickness. Figure S13: Transparency of CuSCN ST-PSCs.

AUTHOR INFORMATION

Corresponding Author

*Email: annalisa@ntu.edu.sg; nripan@ntu.edu.sg

ORCID

Hao Wang: 0000-0003-0037-4523

Herlina Arianita Dewi: 0000-0002-0554-8433

Teck Ming Koh: 0000-0002-2746-3422

Annalisa Bruno: 0000-0002-6963-1682

Subodh Mhaisalkar: 0000-0002-9895-2426

Nripan Mathews: 0000-0001-5234-0822

Notes

Two of the authors, Subodh Mhaisalkar and Nripan Mathews, serve as directors of Prominence Photovoltaics Pte Ltd.

ACKNOWLEDGMENT

We acknowledge Asim Gucchait for his help with the preparation of the initial CuSCN ST-PSCs and Krishnamoorthy Thirumal for PESA measurements. This research is supported by the National Research Foundation, Prime Minister's Office, Singapore under the Intra-CREATE Collaborative Grant (NRF2018-ITC001-001), the Competitive Research Program (NRF-CRP14-2014-03), EIRP (NRF-2015-EWT-EIRP003-004) and Solar CRP (S18-1176-SCRP). The authors would also like to acknowledge funding from Office of Naval Research Global (ONRG-NICOP-N62909-17-1-2155).

REFERENCES

1. Xue, Q.; Xia, R.; Brabec, C. J.; Yip, H.-L., Recent Advances in Semi-transparent Polymer and Perovskite Solar Cells for Power Generating Window Applications. *Energy & Environmental Science* **2018,** *11* (7), 1688-1709.
2. Zhang, W.; Anaya, M.; Lozano, G.; Calvo, M. E.; Johnston, M. B.; Míguez, H.; Snaith, H. J., Highly Efficient Perovskite Solar Cells with Tunable Structural Color. *Nano Letters* **2015,** *15* (3), 1698-1702.
3. (a) https://www.nrel.gov/pv/cell-efficiency.html; (b) Jeon, N. J.; Na, H.; Jung, E. H.; Yang, T.-Y.; Lee, Y. G.; Kim, G.; Shin, H.-W.; Il Seok, S.; Lee, J.; Seo, J., A Fluorene-terminated Hole-transporting Material for Highly Efficient and Stable Perovskite Solar Cells. *Nature Energy* **2018,** *3* (8), 682-689.
4. Shen, H.; Duong, T.; Peng, J.; Jacobs, D.; Wu, N.; Gong, J.; Wu, Y.; Karuturi, S. K.; Fu, X.; Weber, K.; Xiao, X.; White, T. P.; Catchpole, K., Mechanically-stacked Perovskite/CIGS Tandem Solar Cells with Efficiency of 23.9% and Reduced Oxygen Sensitivity. *Energy & Environmental Science* **2018,** *11* (2), 394-406.
5. (a) Snaith, H. J., Perovskites: The Emergence of a New Era for Low-Cost, High-Efficiency Solar Cells. *J. Phys. Chem. Lett.* **2013,** *4* (21), 3623-3630; (b) Service, R. F., Perovskite Solar Cells Gear up to Go Commercial. *Science* **2016,** *354* (6317), 1214-1215.
6. (a) Della Gaspera, E.; Peng, Y.; Hou, Q.; Spiccia, L.; Bach, U.; Jasieniak, J. J.; Cheng, Y.-B., Ultra-thin High Efficiency Semitransparent Perovskite Solar Cells. *Nano Energy* **2015,** *13*, 249-257; (b) Imran, H.; Durrani, I.; Kamran, M.; Abdolkader, T. M.; Faryad, M.; Butt, N. Z., High-Performance Bifacial Perovskite/Silicon Double-Tandem Solar Cell. *IEEE Journal of Photovoltaics* **2018,** *8* (5), 1222-1229; (c) Asadpour, R.; Chavali, R. V. K.; Khan, M. R.; Alam, M. A., Bifacial Si Heterojunction-perovskite Organic-inorganic Tandem to Produce Highly Efficient (ηT* ∼ 33%) Solar Cell. *Applied Physics Letters* **2015,** *106* (24), 243902.
7. Gao, L.; Zhao, E.; Yang, S.; Wang, L.; Li, Y.; Zhao, Y.; Ma, T. In *Light Engineering for Bifacial Transparent Perovskite Solar Cells with High Performance*, SPIE: 2017; p 6.
8. (a) Pang, S.; Li, X.; Dong, H.; Chen, D.; Zhu, W.; Chang, J.; Lin, Z.; Xi, H.; Zhang, J.; Zhang, C.; Hao, Y., Efficient Bifacial Semitransparent Perovskite Solar Cells Using Ag/V2O5 as Transparent Anodes. *ACS Applied Materials & Interfaces* **2018,** *10* (15), 12731-12739; (b) Chen, D.; Pang, S.; Zhu, W.; Zhang, H.;

Zhou, L.; He, F.; Chang, J.; Lin, Z.; Xi, H.; Zhang, J.; Zhang, C.; Hao, Y., Efficient Semitransparent Perovskite Solar Cells Using a Transparent Silver Electrode and Four-Terminal Perovskite/Silicon Tandem Device Exploration. *Journal of Nanomaterials* **2018,** *2018*, 8.
9. Chen, B.; Bai, Y.; Yu, Z.; Li, T.; Zheng, X.; Dong, Q.; Shen, L.; Boccard, M.; Gruverman, A.; Holman, Z.; Huang, J., Efficient Semitransparent Perovskite Solar Cells for 23.0%-Efficiency Perovskite/Silicon Four-Terminal Tandem Cells. *Advanced Energy Materials* **2016,** *6* (19), 1601128.
10. (a) Bailie, C. D.; Christoforo, M. G.; Mailoa, J. P.; Bowring, A. R.; Unger, E. L.; Nguyen, W. H.; Burschka, J.; Pellet, N.; Lee, J. Z.; Grätzel, M.; Noufi, R.; Buonassisi, T.; Salleo, A.; McGehee, M. D., Semi-transparent Perovskite Solar Cells for Tandems with Silicon and CIGS. *Energy & Environmental Science* **2015,** *8* (3), 956-963; (b) Ramírez Quiroz, C. O.; Shen, Y.; Salvador, M.; Forberich, K.; Schrenker, N.; Spyropoulos, G. D.; Heumüller, T.; Wilkinson, B.; Kirchartz, T.; Spiecker, E.; Verlinden, P. J.; Zhang, X.; Green, M. A.; Ho-Baillie, A.; Brabec, C. J., Balancing Electrical and Optical Losses for Efficient 4-terminal Si–perovskite Solar Cells with Solution Processed Percolation Electrodes. *Journal of Materials Chemistry A* **2018,** *6* (8), 3583-3592; (c) Lee, M.; Park, S. J.; Hwang, Y. J.; Jun, Y.; Min, B. K., Tandem Architecture of Perovskite and Cu(In,Ga)(S,Se)2 Created by Solution Processes for Solar Cells. *Advanced Optical Materials* **2016,** *4* (12), 2102-2108.
11. Lang, F.; Gluba, M. A.; Albrecht, S.; Rappich, J.; Korte, L.; Rech, B.; Nickel, N. H., Perovskite Solar Cells with Large-Area CVD-Graphene for Tandem Solar Cells. *J. Phys. Chem. Lett.* **2015,** *6* (14), 2745-2750.
12. Zhang, Y.; Wu, Z.; Li, P.; Ono, L. K.; Qi, Y.; Zhou, J.; Shen, H.; Surya, C.; Zheng, Z., Fully Solution-Processed TCO-Free Semitransparent Perovskite Solar Cells for Tandem and Flexible Applications. *Advanced Energy Materials* **2018,** *8* (1), 1701569.
13. (a) Zhao, D.; Yu, Y.; Wang, C.; Liao, W.; Shrestha, N.; Grice, C. R.; Cimaroli, A. J.; Guan, L.; Ellingson, R. J.; Zhu, K.; Zhao, X.; Xiong, R.-G.; Yan, Y., Low-bandgap Mixed Tin–lead Iodide Perovskite Absorbers with Long Carrier Lifetimes for All-perovskite Tandem Solar Cells. *Nature Energy* **2017,** *2*, 17018; (b) Yang, Y.; Chen, Q.; Hsieh, Y.-T.; Song, T.-B.; Marco, N. D.; Zhou, H.; Yang, Y., Multilayer Transparent Top Electrode for Solution Processed Perovskite/Cu(In,Ga)(Se,S)2 Four Terminal Tandem Solar Cells. *ACS Nano* **2015,** *9* (7), 7714-7721.
14. (a) McMeekin, D. P.; Sadoughi, G.; Rehman, W.; Eperon, G. E.; Saliba, M.; Hörantner, M. T.; Haghighirad, A.; Sakai, N.; Korte, L.; Rech, B.; Johnston, M. B.; Herz, L. M.; Snaith, H. J., A Mixed-Cation Lead Mixed-halide Perovskite Absorber for Tandem Solar Cells. *Science* **2016,** *351* (6269), 151-155; (b) Werner, J.; Barraud, L.; Walter, A.; Bräuninger, M.; Sahli, F.; Sacchetto, D.; Tétreault, N.; Paviet-Salomon, B.; Moon, S.-J.; Allebé, C.; Despeisse, M.; Nicolay, S.; De Wolf, S.; Niesen, B.; Ballif, C., Efficient Near-Infrared-Transparent Perovskite Solar Cells Enabling Direct Comparison of 4-Terminal and Monolithic Perovskite/Silicon Tandem Cells. *ACS Energy Letters* **2016,** *1* (2), 474-480; (c) Bush, K. A.; Bailie, C. D.; Chen, Y.; Bowring, A. R.; Wang, W.; Ma, W.; Leijtens, T.; Moghadam, F.; McGehee, M. D., Thermal and Environmental Stability of Semi-Transparent Perovskite Solar Cells for Tandems Enabled by a Solution-Processed Nanoparticle Buffer Layer and Sputtered ITO Electrode. *Advanced Materials* **2016,** *28* (20), 3937-3943; (d) Kanda, H.; Uzum, A.; Nishino, H.; Umeyama, T.; Imahori, H.; Ishikawa, Y.; Uraoka, Y.; Ito, S., Interface Optoelectronics Engineering for Mechanically Stacked Tandem Solar Cells Based on Perovskite and Silicon. *ACS Applied Materials & Interfaces* **2016,** *8* (49), 33553-33561; (e) Duong, T.; Wu, Y.; Shen, H.; Peng, J.; Fu, X.; Jacobs, D.; Wang, E.-C.; Kho, T. C.; Fong, K. C.; Stocks, M.; Franklin, E.; Blakers, A.; Zin, N.; McIntosh, K.; Li, W.; Cheng, Y.-B.; White, T. P.; Weber, K.; Catchpole, K., Rubidium Multication Perovskite with Optimized Bandgap for Perovskite-Silicon Tandem with over 26% Efficiency. *Advanced Energy Materials* **2017,** *7* (14), 1700228; (f) Guchhait, A.; Dewi, H. A.; Leow, S. W.; Wang, H.; Han, G.; Suhaimi, F. B.; Mhaisalkar, S.; Wong, L. H.; Mathews, N., Over 20% Efficient CIGS–Perovskite Tandem Solar Cells. *ACS Energy Letters* **2017,** *2* (4), 807-812; (g) Zhao, D.; Wang, C.; Song, Z.; Yu, Y.;

Chen, C.; Zhao, X.; Zhu, K.; Yan, Y., Four-Terminal All-Perovskite Tandem Solar Cells Achieving Power Conversion Efficiencies Exceeding 23%. *ACS Energy Letters* **2018,** *3* (2), 305-306.
15. (a) Werner, J.; Dubuis, G.; Walter, A.; Löper, P.; Moon, S.-J.; Nicolay, S.; Morales-Masis, M.; De Wolf, S.; Niesen, B.; Ballif, C., Sputtered Rear Electrode with Broadband Transparency for Perovskite Solar Cells. *Solar Energy Materials and Solar Cells* **2015,** *141*, 407-413; (b) Wahl, T.; Hanisch, J.; Meier, S.; Schultes, M.; Ahlswede, E., Sputtered Indium Zinc Oxide Rear Electrodes for Inverted Semitransparent Perovskite Solar Cells without Using a Protective Buffer Layer. *Organic Electronics* **2018,** *54*, 48-53; (c) Yu-Hsien, C.; Chieh-Chung, P.; Yu-Hung, C.; Yung-Liang, T.; Song-Yeu, T.; Peter, C., The Utilization of IZO Transparent Conductive Oxide for Tandem and Substrate Type Perovskite Solar Cells. *Journal of Physics D: Applied Physics* **2018,** *51* (42), 424002.
16. Fu, F.; Pisoni, S.; Weiss, T. P.; Feurer, T.; Wäckerlin, A.; Fuchs, P.; Nishiwaki, S.; Zortea, L.; Tiwari, A. N.; Buecheler, S., Compositionally Graded Absorber for Efficient and Stable Near-Infrared-Transparent Perovskite Solar Cells. *Advanced Science* **2018,** *5* (3), 1700675.
17. Li, Y.; Duan, J.; Zhao, Y.; Tang, Q., All-inorganic Bifacial CsPbBr3 Perovskite Solar Cells with a 98.5%-Bifacial Factor. *Chemical Communications* **2018,** *54* (59), 8237-8240.
18. (a) Madhavan, V. E.; Zimmermann, I.; Roldán-Carmona, C.; Grancini, G.; Buffiere, M.; Belaidi, A.; Nazeeruddin, M. K., Copper Thiocyanate Inorganic Hole-Transporting Material for High-Efficiency Perovskite Solar Cells. *ACS Energy Letters* **2016,** *1* (6), 1112-1117; (b) Ye, S.; Sun, W.; Li, Y.; Yan, W.; Peng, H.; Bian, Z.; Liu, Z.; Huang, C., CuSCN-Based Inverted Planar Perovskite Solar Cell with an Average PCE of 15.6%. *Nano Letters* **2015,** *15* (6), 3723-3728; (c) Murugadoss, G.; Thangamuthu, R.; Senthil Kumar, S. M., Fabrication of CH3NH3PbI3 Perovskite-based Solar Cells: Developing Various New Solvents for CuSCN Hole Transport Material. *Solar Energy Materials and Solar Cells* **2017,** *164*, 56-62.
19. (a) Jung, M.; Kim, Y. C.; Jeon, N. J.; Yang, W. S.; Seo, J.; Noh, J. H.; Il Seok, S., Thermal Stability of CuSCN Hole Conductor-Based Perovskite Solar Cells. *ChemSusChem* **2016,** *9* (18), 2592-2596; (b) Zhao, K.; Munir, R.; Yan, B.; Yang, Y.; Kim, T.; Amassian, A., Solution-processed Inorganic Copper(i) Thiocyanate (CuSCN) Hole Transporting Layers for Efficient p-i-n Perovskite Solar Cells. *Journal of Materials Chemistry A* **2015,** *3* (41), 20554-20559.
20. (a) Arora, N.; Dar, M. I.; Hinderhofer, A.; Pellet, N.; Schreiber, F.; Zakeeruddin, S. M.; Grätzel, M., Perovskite solar cells with CuSCN hole extraction layers yield stabilized efficiencies greater than 20%. *Science* **2017,** *358* (6364), 768-771; (b) Jung, J. W.; Chueh, C.-C.; Jen, A. K.-Y., High-Performance Semitransparent Perovskite Solar Cells with 10% Power Conversion Efficiency and 25% Average Visible Transmittance Based on Transparent CuSCN as the Hole-Transporting Material. *Advanced Energy Materials* **2015,** *5* (17), 1500486.
21. Fan, L.; Li, Y.; Yao, X.; Ding, Y.; Zhao, S.; Shi, B.; Wei, C.; Zhang, D.; Li, B.; Wang, G.; Zhao, Y.; Zhang, X., Delayed Annealing Treatment for High-Quality CuSCN: Exploring Its Impact on Bifacial Semitransparent n-i-p Planar Perovskite Solar Cells. *ACS Applied Energy Materials* **2018,** *1* (4), 1575-1584.
22. Deng, Y.; Wang, Q.; Yuan, Y.; Huang, J., Vividly Colorful Hybrid Perovskite Solar Cells by Doctor-blade Coating with Perovskite Photonic Nanostructures. *Materials Horizons* **2015,** *2* (6), 578-583.
23. Lee, K.-T.; Jang, J.-Y.; Zhang, J.; Yang, S.-M.; Park, S.; Park, H. J., Highly Efficient Colored Perovskite Solar Cells Integrated with Ultrathin Subwavelength Plasmonic Nanoresonators. *Scientific Reports* **2017,** *7* (1), 10640.
24. Schlisske, S.; Mathies, F.; Busko, D.; Strobel, N.; Rödlmeier, T.; Richards, B. S.; Lemmer, U.; Paetzold, U. W.; Hernandez-Sosa, G.; Klampaftis, E., Design and Color Flexibility for Inkjet-Printed Perovskite Photovoltaics. *ACS Applied Energy Materials* **2019,** *2* (1), 764-769.
25. Upama, M. B.; Mahmud, M. A.; Yi, H.; Elumalai, N. K.; Conibeer, G.; Wang, D.; Xu, C.; Uddin, A., Low-temperature Processed Efficient and Colourful Semitransparent Perovskite Solar Cells for Building Integration and Tandem Applications. *Organic Electronics* **2019,** *65*, 401-411.

26. Lee, K.-T.; Fukuda, M.; Joglekar, S.; Guo, L. J., Colored, See-through Perovskite Solar Cells Employing an Optical Cavity. *Journal of Materials Chemistry C* **2015,** *3* (21), 5377-5382.
27. Lu, J.-H.; Yu, Y.-L.; Chuang, S.-R.; Yeh, C.-H.; Chen, C.-P., High-Performance, Semitransparent, Easily Tunable Vivid Colorful Perovskite Photovoltaics Featuring Ag/ITO/Ag Microcavity Structures. *The Journal of Physical Chemistry C* **2016,** *120* (8), 4233-4239.
28. Lee, K.-T.; Jang, J.-Y.; Ha, N. Y.; Lee, S.; Park, H. J., High-performance Colorful Semitransparent Perovskite Solar Cells with Phase-compensated Microcavities. *Nano Research* **2018,** *11* (5), 2553-2561.
29. Lee, K.-T.; Jang, J.-Y.; Park, S. J.; Ok, S. A.; Park, H. J., Incident-angle-controlled Semitransparent Colored Perovskite Solar Cells with Improved Efficiency Exploiting a Multilayer Dielectric Mirror. *Nanoscale* **2017,** *9* (37), 13983-13989.
30. Jiang, Y.; Luo, B.; Jiang, F.; Jiang, F.; Fuentes-Hernandez, C.; Liu, T.; Mao, L.; Xiong, S.; Li, Z.; Wang, T.; Kippelen, B.; Zhou, Y., Efficient Colorful Perovskite Solar Cells Using a Top Polymer Electrode Simultaneously as Spectrally Selective Antireflection Coating. *Nano Letters* **2016,** *16* (12), 7829-7835.
31. Guerrero-Lemus, R.; Vega, R.; Kim, T.; Kimm, A.; Shephard, L. E., Bifacial Solar Photovoltaics – A Technology Review. *Renewable and Sustainable Energy Reviews* **2016,** *60*, 1533-1549.
32. Saliba, M.; Matsui, T.; Seo, J.-Y.; Domanski, K.; Correa-Baena, J.-P.; Nazeeruddin, M. K.; Zakeeruddin, S. M.; Tress, W.; Abate, A.; Hagfeldt, A.; Gratzel, M., Cesium-containing Triple Cation Perovskite Solar Cells: Improved Stability, Reproducibility and High Efficiency. *Energy & Environmental Science* **2016,** *9* (6), 1989-1997.
33. Fu, F.; Feurer, T.; Jäger, T.; Avancini, E.; Bissig, B.; Yoon, S.; Buecheler, S.; Tiwari, A. N., Low-temperature-processed Efficient Semi-transparent Planar Perovskite Solar Cells for Bifacial and Tandem Applications. *Nature Communications* **2015,** *6*, 8932.
34. Jin, J.-M., *The Finite Element Method in Electromagnetics, 2nd Edition*. 2nd ed.; Wiley-IEEE Press: New York, 2002; p 780.
35. Kwon, H.-C.; Kim, A.; Lee, H.; Lee, D.; Jeong, S.; Moon, J., Parallelized Nanopillar Perovskites for Semitransparent Solar Cells Using an Anodized Aluminum Oxide Scaffold. *Advanced Energy Materials* **2016,** *6* (20), 1601055.
36. Ball, J. M.; Stranks, S. D.; Hörantner, M. T.; Hüttner, S.; Zhang, W.; Crossland, E. J. W.; Ramirez, I.; Riede, M.; Johnston, M. B.; Friend, R. H.; Snaith, H. J., Optical Properties and Limiting Photocurrent of Thin-film Perovskite Solar Cells. *Energy & Environmental Science* **2015,** *8* (2), 602-609.
37. Löper, P.; Stuckelberger, M.; Niesen, B.; Werner, J.; Filipič, M.; Moon, S.-J.; Yum, J.-H.; Topič, M.; De Wolf, S.; Ballif, C., Complex Refractive Index Spectra of CH3NH3PbI3 Perovskite Thin Films Determined by Spectroscopic Ellipsometry and Spectrophotometry. *J. Phys. Chem. Lett.* **2015,** *6* (1), 66-71.
38. Auer-Berger, M.; Tretnak, V.; Wenzl, F.-P.; Krenn, J. R.; List-Kratochvil, E. J. W., Adjusting the Emission Color of Organic Light-emitting Diodes through Aluminum Nanodisc Arrays. *Optical Engineering* **2017,** *56* (9), 097102.
39. Holman, Z. C.; Filipič, M.; Descoeudres, A.; Wolf, S. D.; Smole, F.; Topič, M.; Ballif, C., Infrared Light Management in High-efficiency Silicon Heterojunction and Rear-passivated Solar Cells. *Journal of Applied Physics* **2013,** *113* (1), 013107.

TOC GRAPHICS

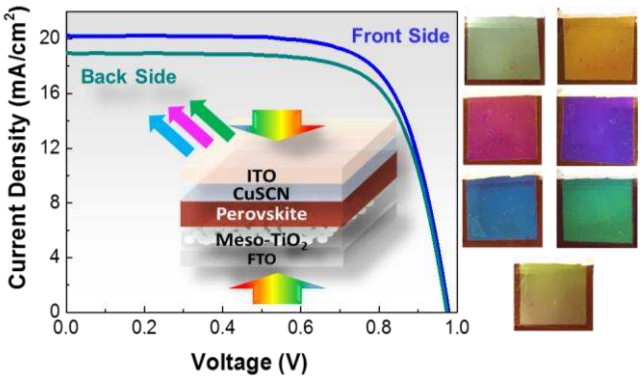
Front Side
Back Side
ITO
CuSCN
Perovskite
Meso-TiO2
FTO
Current Density (mA/cm2)
Voltage (V)
0
4
8
12
16
20
0.0
0.2
0.4
0.6
0.8
1.0